Cancer Science
Japanese Cancer Association JCA
Open Access

Identification of anti-cancer chemical compounds using Xenopus embryos

Masamitsu Tanaka,[1] Sei Kuriyama,[1] Go Itoh,[1] Aki Kohyama,[2] Yoshiharu Iwabuchi,[2] Hiroyuki Shibata,[3] Masakazu Yashiro[4] and Namiko Aiba[1]

[1]Department of Molecular Medicine and Biochemistry, Akita University Graduate School of Medicine, Akita; [2]Department of Organic Chemistry, Graduate School of Pharmaceutical Sciences, Tohoku University, Sendai; [3]Department of Clinical Oncology, Akita University Graduate School of Medicine, Akita; [4]Department of Surgical Oncology, Osaka City University Graduate School of Medicine, Osaka, Japan

Key words

Chemical screening, development, microtubule, tumor invasion, Xenopus

Correspondence

Masamitsu Tanaka, Department of Molecular Medicine and Biochemistry, Akita University Graduate School of Medicine, 1-1-1 Hondo, Akita 010-8543, Japan.
Tel: +81-018-884-6077; Fax: +81-018-884-6078;
E-mail: mastanak@med.akita-u.ac.jp

Funding Information

This work was supported by JST KAKENHI (Grant Nos. 25290042, 26640068; 15K06822), JST A-STEP (AS262Z01408Q) and MEXT KAKENHI (25111702).

Received December 14, 2015; Revised March 22, 2016; Accepted March 28, 2016

Cancer Sci **107** (2016) 803–811

doi: 10.1111/cas.12940

Cancer tissues have biological characteristics similar to those observed in embryos during development. Many types of cancer cells acquire pro-invasive ability through epithelial–mesenchymal transition (EMT). Similar processes (gastrulation and migration of cranial neural crest cells [CNCC]) are observed in the early stages of embryonic development in Xenopus during which cells that originate from epithelial sheets through EMT migrate to their final destinations. The present study examined Xenopus embryonic tissues to identify anti-cancer compounds that prevent cancer invasion. From the initial test of known anti-cancer drugs, AMD3100 (an inhibitor of CXCR4) and paclitaxel (a cytoskeletal drug targeting microtubules) effectively prevented migration during gastrulation or CNCC development. Blind-screening of 100 synthesized chemical compounds was performed, and nine candidates that inhibited migration of these embryonic tissues without embryonic lethality were selected. Of these, C-157 (an analog of podophyllotoxin) and D-572 (which is an indole alkaroid) prevented cancer cell invasion through disruption of interphase microtubules. In addition, these compounds affected progression of mitotic phase and induced apoptosis of SAS oral cancer cells. SAS tumors were reduced in size after intratumoral injection of C-157, and peritoneal dissemination of melanoma cells and intracranial invasion of glioma cells were inhibited by C-157 and D-572. When the other analogues of these chemicals were compared, those with subtle effect on embryos were not tumor suppressive. These results suggest that a novel chemical-screening approach based on Xenopus embryos is an effective method for isolating anti-cancer drugs and, in particular, targeting cancer cell invasion and proliferation.

In vivo screening of anti-tumor chemical compounds is advantageous in that the process can identify compounds that effectively suppress tumors without severe side-effects. However, *in vivo* screening based on assays that evaluate tumorigenicity or metastasis of cancer cells in mice is complex and time-consuming. To overcome such problems, we developed an assay based on embryonic development, which shares biological features with cancer tissues.

In vertebrate embryos during early development (e.g. gastrulation and migration of neural crest cells [NCC]), cells originated from epithelial cells cause EMT, and become highly invasive. They often migrate and invade as a group of cells. In many cancers, cancer cells invade the stromal tissues and vessels along with EMT to establish metastatic colonies.[1–3] Thus, we used frog embryos to identify compounds that inhibit cancer invasion and metastasis. We chose frog embryos because they develop quickly and the cell behaviors of gastrulation and NCC are well understood.[4] The Xenopus system can contributes to the understanding of tumor biology and pathogenesis.[5] Despite the fact that the primary amino acid sequences of frog molecules are different from those in mammals, many mammalian constructs show functional homology, and chemical compounds such as the MEK inhibitor, U0126, affect MEK function both in frog and mammalian cells.[6,7]

Gastrulation establishes the basic vertebrate body plan, leading to the formation of the three distinct germ layers. During gastrulation, mesodermal cells emerge from the epidermis through EMT through the activation of TGF-ß signaling,[8] and migrate from posterior to anterior (Fig. S1a). The leader cells, called leading edge mesoendoderm (LEM), are present in the most anterior fraction of the migrating mesodermal cells, and the migration of these cells seems to depend on chemotaxis driven by the SDF1/CXCR4 interaction (Fig. S1a),[9] the signaling for which is also activated by EMT in various cancer cells.[10–14] During gastrulation, SDF-1 is present in the blastocoel roof, which provides extracellular substrates through which the LEM migrates toward the anterior region.[15,16]

Cranial neural crest cells (CNCC) are a transient, migratory and invasive population during embryogenesis. These cells emerge from the ectoderm and differentiate into bone, cartilage and melanocyte after migration.[17–19] The NCC marker, Snail1/2, regulates EMT in cancer.[20] Xenopus CNCC are

used as a model system of cell migration, which is also regulated by SDF-1/CXCR4 signaling.[21–23]

Here, we used Xenopus embryos to screen 100 synthesized chemical compounds that prevented gastrulation or migration of CNCC. We eliminated the compounds that caused embryonic death due to severe toxicity or induction of developmental defects in multiple organs. Among the compounds obtained from this screening, two compounds suppressed invasion by several cancer cell lines. These two compounds disturbed microtubule formation and, therefore, affected both migration and proliferation of cancer cells. From several known anti-cancer drugs, paclitaxel, which also targets microtubules, and an inhibitor of CXCR4 similarly prevented these embryonic events. Thus, our chemical screening method using Xenopus embryos is an attractive tool for identification of anti-cancer agents targeting invasion and proliferation based on various mechanisms.

Materials and Methods

Cell lines and culture. SAS, a squamous cell carcinoma cell line derived from the oral cavity, B16 mouse melanoma cells and C6 rat glioma cells were obtained from the American Type Culture Collection. These cancer cells were cultured in DMEM containing 1.0 g/L glucose, 10% FBS and penicillin–streptomycin (Sigma, St. Louis, MO, USA). Axcel cells were established from metastatic lesions of melanoma patients[4] and cultured in RPMI-1640 (Sigma) containing 10% FBS. Cancer-associated fibroblasts (CAF) were obtained from the tumoral gastric wall and cultured in DMEM containing 4.5 g/L glucose and 10% FBS.[24]

Chemical compounds and reagents. A total of 100 chemical compounds were selected from the synthetic compound library accumulated in the Department of Organic Chemistry, Graduate School of Pharmaceutical Sciences, Tohoku University (see Data S1). The following anti-cancer drugs were purchased: Sunitinib (Sigma-Aldrich, St. Louis, MO, USA), Sorafenib (LC Laboratories, Woburn, MA, USA), Paclitaxel (Merck Millipore, Darmstadt, Germany) and AMD3100 (Wako Pure Chemical Industries, Osaka, JAPAN). The following antibodies were purchased: anti-Erk, phosphor-Erk Thr202/Tyr204, Akt and phosphor-Akt Thr388 (Cell Signaling Technology, Danvers, MA, USA), anti α-tubulin antibody (Santa Cruz, Dallas, Texas, USA) and Alexa-Fluor-488 Goat Anti-Mouse IgG (Life Technologies, Rockville, MD, USA). 3,3′-dioctadecycloxacarbo-cyanine perchlorate (DiO) and 1,1′-dioctadecyl-3,3,3′,3′-tetramethyllindo-carbocyanine perchlorate (DiI) were purchased from Thermo Fisher Scientific (Waltham, MA, USA).

Xenopus embryo manipulation. Xenopus laevis were purchased from Watanabe-Zoushoku (Hyogo, Japan). Eggs were obtained from females after human gonadotropin-induced spawning and stored in 1 × Marc's Modified Ringers (MMR) buffer (0.1 M NaCl, 2 mM KCl, 1 mM MgSO4, 2 mM CaCl2, 5 mM HEPES [pH 7.8], 0.1 mM EDTA) until required.[25] The eggs were fertilized *in vitro* and dejellied by exposure to 1% cystein hydrochloride in 0.3 × MMR. Healthy embryos were selected at the cleavage stage (32 cells). Vitelline membranes were removed by forceps manually at the end of the blastula stage, and the embryos (stage 10) were treated with 50 μM of each chemical compound. The gastrulation defect was evaluated when the control embryos reached stage 12.5 or 14. For the CNCC assay, the fertilized embryos were kept in 0.1× MMR until stage 17 before the vitelline membranes were removed in 1× MMR. The embryos were treated with 50 μM of each chemical compound in 0.5× MMR overnight at 14.5°C, and then fixed at several time-points thereafter.

Whole-mount in situ hybridization. Embryos were fixed in fresh 1× MEMFA for 1.5 h, and washed in 50% MeOH, 100% MeOH and absolute EtOH, and then stored at −20°C. *In situ* hybridization was performed as previously described.[26] As a first round, we put 3–5 different pools of embryos treated with each compounds into a single vial together, to make sure that the staining steps were uniformly performed. Next, when we found irregular migration patterns in some vial, we performed *in situ* hybridization for 3–5 different compounds individually. Finally, we selected the particular compound when the first and the second rounds of phenotypes were identical to avoid the possibility that the first screening contained any natural developmental errors.

3D gel invasion assay. The assay was performed as described previously.[27] Briefly, cancer cells and fibroblasts (2×10^4 of each) were mixed and placed on gels containing type-I collagen and Matrigel. In another gel invasion assay, fibroblasts were embedded in a gel that was then overlaid with cancer cells. The gels were fixed, vertically cut into 200-μm slices, and visualized under a confocal microscope (LSM780; Zeiss, Oberkochen, Germany). The area invaded by the cells was quantified using ImageJ software (NIH, Bethesda, MD, USA).[27] The invasion index (I) was calculated as the ratio of the area invaded by the test cells to that invaded by control cells.

Apoptosis and MTT assays. SAS cells were plated onto 96-well plates in triplicate and cultured in DMEM containing 10% FBS. Cells were treated with each chemical for 12 h, and tested in apoptosis and MTT assays. For the apoptosis assay, cells were lysed and nucleosomes in the cytoplasm of apoptotic cells were measured using a Cell Death enzyme-linked immunosorbent assay kit (Roche, Mannheim, Germany). The MTT assay was performed using a CellQuanti-MTT cell viability assay kit (BioAssay Systems, Hayward, CA, USA). In some experiments, apoptosis was also detected by labeling cells with Hoechst 33342 using NucBlue Live Ready Probes (Life Technologies).

Immunofluorescence. SAS cells grown on coverslips were treated with 0.01% DMSO, 10 μM C-157 or D-572 for 12 h and fixed with methanol for 10 min. Cells were incubated with anti-α-tubulin antibody for 3 h at room temperature, followed by incubation with Alexa-Fluor-488 Goat Anti-Mouse IgG for 1 h.

Mouse experiments. All animal experiments were approved by the Committee for Ethics of Animal Experimentation, and the experiments were conducted in accordance with the guidelines for animal experiments at Akita University. For the *in vivo* tumor implantation assays, SAS cells (1.5×10^6) were injected subcutaneously into the right flank of 6-week-old BALB/c nude mice (CLEA Japan, Tokyo, Japan). Test chemicals were injected into the tumors every other day. Mice were killed 9 days after subcutaneous injection of tumor cells. Peritoneal dissemination was examined by intraperitoneal injection of Axcel cells (5×10^6) suspended in 300 μL of medium. Mice were killed 20 days after injection. Invasion into the brain was tested by intracranial injection of C6 glioma cells (2×10^5) suspended in 30 μL of medium into 6-week-old BALB/c nude mice. Five mice per group were examined.

Statistical analysis. Statistical significance was calculated using Student's *t*-test. *P*-values < 0.05 were considered significant.

Results

***In vivo* screening of chemicals perturbing cell migration of Xenopus embryos.** During gastrulation, mesodermal cells,

which originated from the epidermis through EMT, lost their association with the overlying epithelium and moved inward to the blastopore (a small hole in the vegetal region of the embryo) from where they began their migration upward and across the roof of the blastocoel (Figs 1a, S1a). As gastrulation proceeded, the lower edge of the ectodermal tissue converged and constricted circumferentially, closing around the blastopore (stage 12-12 1/2; Fig. 1b,c). Later (at the neurula stage), the blastopore was completely closed (stage 14; Fig. 1g–i).

To examine the effects of chemicals on gastrulation, 10 embryos were put into each well of a 24-well plate, and exposed to each chemical compound blindly (50 μM in buffer) when embryos reached stage 10 (the onset of gastrulation). Embryos were viewed from the vegetal pole when control embryos reached stage 12 1/2 and stage 14, and the degree of blastopore closure was evaluated (Fig. 1d). Typical embryos showing perturbed gastrulation experienced delayed blastopore closure (Figs 1e,f,j,k, S1b, top). Naturally occurring gastrulation defects occurred in <10% of embryos. A compound that attenuated blastopore closure in more than half of embryos was evaluated as positive. Compounds that killed the embryos were eliminated (Fig. S1b, bottom). Five compounds induced gastrulation defects without affecting viability (C-157, D-572, GS05-TS101, D-545 and GO-060) (Figs 1, S1b).

In the second assay based on CNCC, embryos were exposed to chemicals after gastrulation and CNCC migration was analyzed *in vivo* by detecting the CNCC markers FoxD3 and Dlx2 by whole-mount *in situ* hybridization (Fig. 2a). CNCC markers were observed at stages 23, 25 and 30 (before, during and after CNCC migration, respectively). At stage 30, CNCC normally segregate into four streams (mandibular, hyoid, anterior branchial and posterior branchial arches) (Fig. 2b,c: control). Five compounds induced strong (Fig. 2c; GS02-MK033, GS02-KK005, GS05-TS089, GS05-TS147 and D-572), and three compounds induced moderate (Fig. 2d; B-214, C-162 and D-316) migration defects. Except for CNCC, these embryos were of normal appearance without apparent defects in other organs, including eyes and otic vesicles. In all, nine chemical compounds that induced severe defects in either gastrulation or neural crest development were tested further using cancer cell lines.

To evaluate the above strategies, we also examined several known cancer therapeutic drugs. Sunitinib is an inhibitor of multiple receptor tyrosine kinases,[28–30] and Sorafenib also inhibits tyrosine kinases, including B-Raf and VEGF-receptor.[31,32] Both Sunitinib and Sorafenib inhibit angiogenesis in Xenopus embryos,[33] whereas they did not show any significant effect on gastrulation (Fig. S2a–c,f) or neural crest migration (Fig. S2g,h,k). Paclitaxel is a cytoskeletal drug that targets

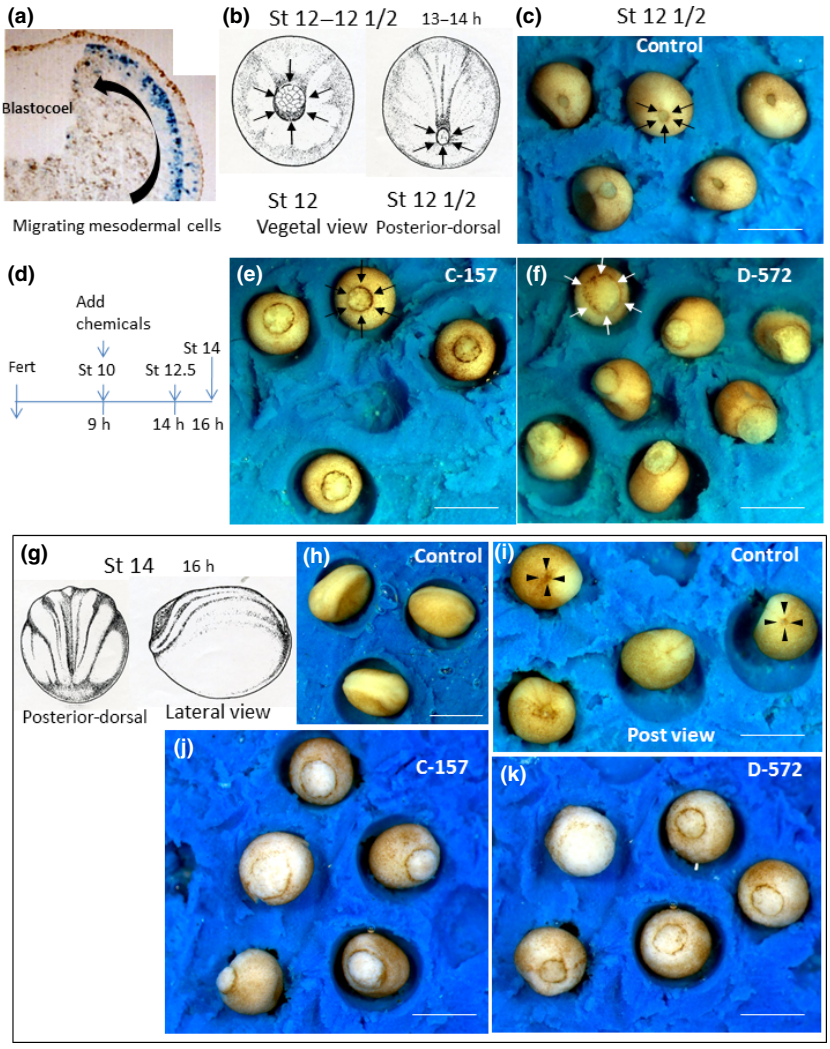

Fig. 1. Screening of chemicals that perturb gastrulation. (a) X-Gal staining of a normal embryo after injection of nuclear-localized β-galactosidase mRNA into dorsal-vegetal blastomeres at the eight-cell stage. Cells stained blue are migrating mesodermal cells.[44] (b) Vegetal or posterior-dorsal views of stage 12–12 1/2 normal embryos (end of gastrulation). Arrows indicate blastopores. (d) Experimental sheme. (c, e, f) stage 12 1/2 embryos treated with 0.05% DMSO (control) or test chemicals (50 μM). (g) Stage 14 normal embryos (neurula stage). (h–k) Embryos at stage 14, treated with 0.05% DMSO (control) or test chemicals (50 μM). Bar = 2 mm.

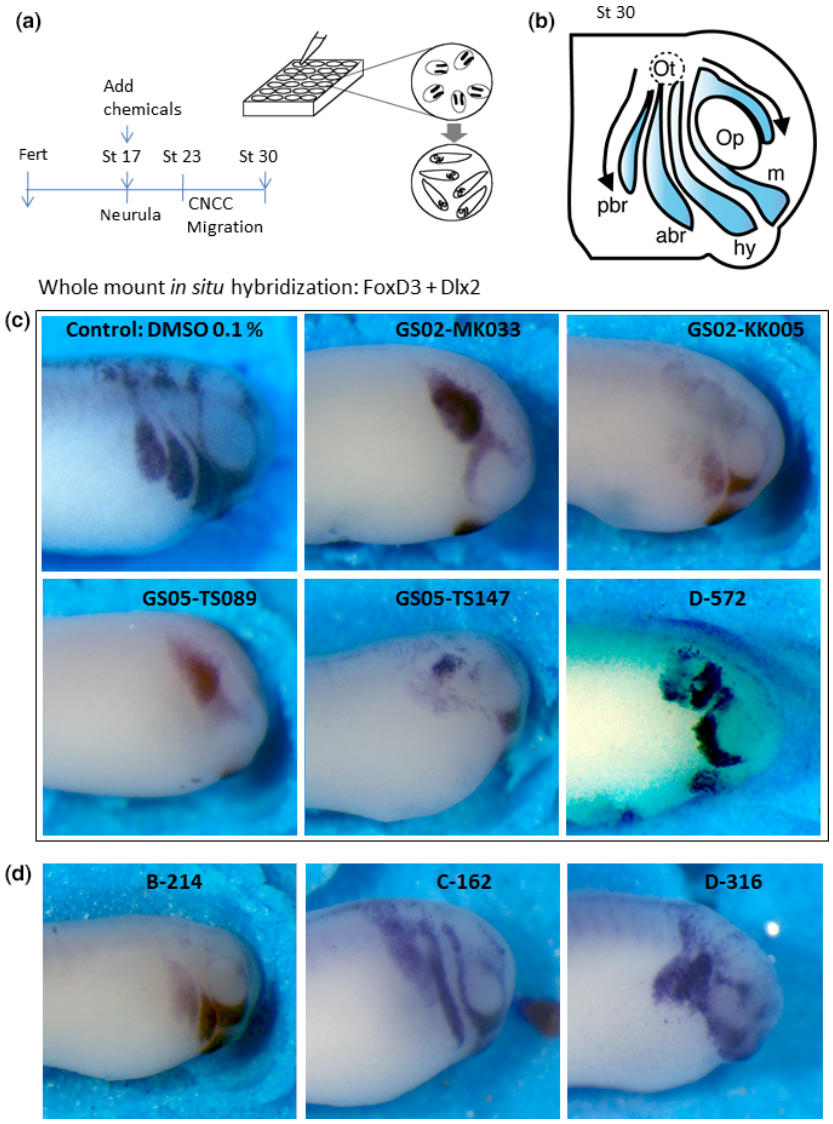

Fig. 2. Screening of chemicals that perturb migration of cranial neural crest cells (CNCC). (a) Experimental scheme. (b) Migratory CNCC streams at the tailbud craniofacial area (stage 30). The blue region indicates CNCC. Arrows indicate the direction of migration. abr, anterior branchial arch; hy, hyoid segment; m, mandibular segment; Op, optic vesicle; Ot, otic vesicle; pbr, posterior branchial arch. (c, d) Whole-mount *in situ* hybridization: FoxD3 is a pre-migratory NCC marker and Dlx2 is a migratory NCC marker. Mixture of these probes indicates whole NCC. DMSO (0.1%) did not affect migratory patterns, which comprised four streams of cranial NCC. (c) Five chemicals induced severe defects in CNCC migration. (d) Three chemicals had relatively mild effects.

microtubules,[34,35] and AMD3100 is an inhibitor of CXCR4, which is involved in SDF1-dependent chemokine signaling.[36] SDF1-CXCR4 signaling is important for the migration during gastrulation and neural crest development.[9,22–24] As expected, both paclitaxel and AMD3100 inhibited blastopore closure, so that the large endodermal bulge remains outside (Fig. S2d–f), and they also affected neural crest migration dose-dependently (Fig. S2i–k). However, there were no significant defects in other organs, such as the central nervous system or body axes (data not shown). These results suggest that the specificity of drug effects in these assays is high, and anti-cancer drugs based on different mechanisms can be selected.

Inhibitory effect of chemicals on cancer cell invasion. Because the cells that migrate during gastrulation and neural crest development are derived from the ectodermal monolayer, SAS cells (derived from a patient of squamous cell carcinoma of the oral cavity) were used for the tests.[37] We also used B16 melanoma cells, as melanocytes develop from migrated NCC.

To examine the effects of candidate compounds on cancer cell invasion, 3D gel invasion assay was performed.[27] In this assay, gel invasion by SAS cells alone or B16 cells alone was very weak (Fig. S3a). Therefore, fibroblasts were mixed with these cancer cells, and the effects of the chemical compounds on coordinated invasion by fibroblasts and cancer cells, which reflects the cancer invasion *in vivo*, were examined. To this end, cells were labeled with distinguishable fluorescent dyes and placed on top of a gel containing extracellular-matrix (ECM) components (Fig. 3a). Clusters of SAS cells and fibroblasts entered into the gel when they were mixed (Fig. 3b). Treatment of the cells with C-157 or D-572 showed significant suppression of invasion (Fig. 3c,d). Weak inhibition of co-invasion by SAS cells and CAF was also observed in the presence of GS02-MK033 (Fig. 3e). None of the other candidate chemicals effectively suppressed invasion by SAS cells and fibroblasts (Figs 3f, S3b). Similarly, C-157 and D-572 inhibited coordinated invasion by B16 melanoma cells and fibroblasts (Fig. S3c).

To further evaluate the migration of SAS cells, we performed another gel invasion assay that resembles invasion of oral cancer into the dermis. First, fibroblasts were embedded in an ECM-gel and SAS cells were plated on top. The area of invading SAS cells in the gel was then quantified (Fig. 3h). In the control, a large number of SAS cells invaded the gel containing fibroblasts. Typically, they invaded as a cluster or as a

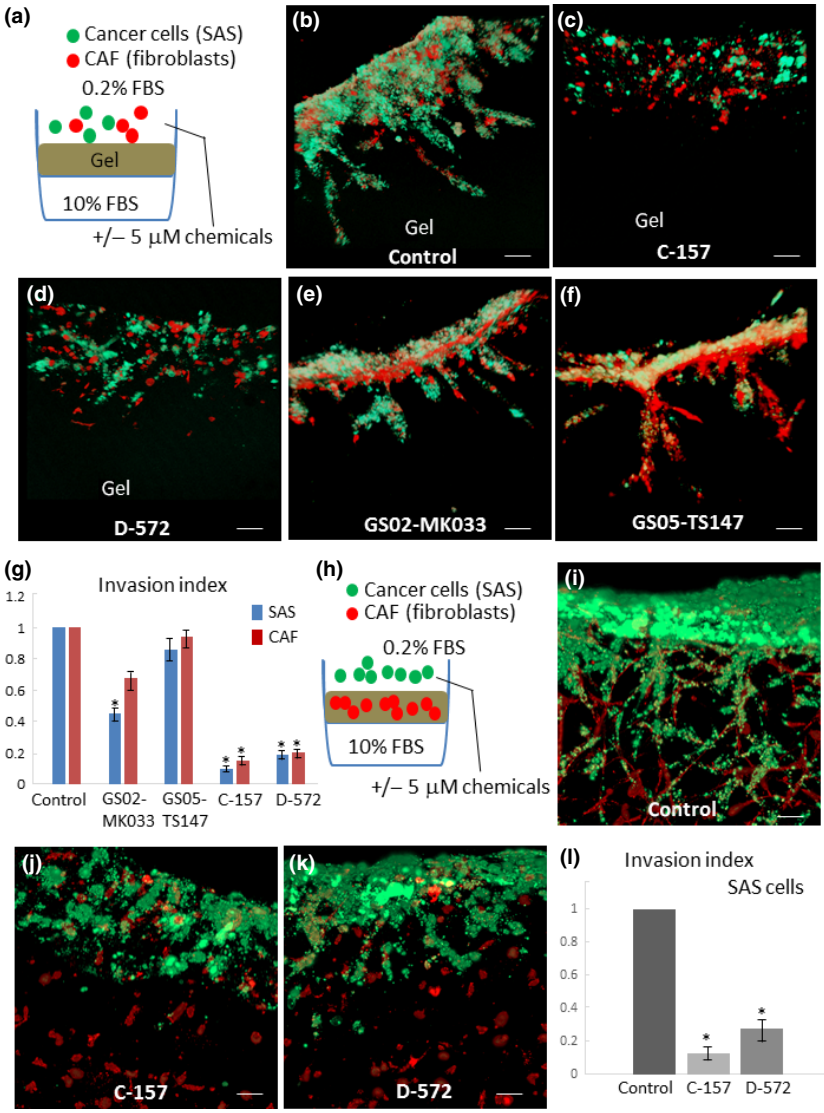

Fig. 3. 3D gel invasion assays. (a) Schematic showing the experiments in b–g. DiO-labeled SAS cells and DiI-labeled cancer-associated fibroblasts (CAF) were mixed and placed onto the gel. (b–f) Representative photos of sectioned gels after 7 days of incubation. (h) Schematic representation of the experiments in i–l. CAF (DiI-labeled, red) were embedded in gels in Transwells with 0.4-μm pores; DiO-labeled (green) SAS cells were then overlaid onto the gels. After incubation for 9 days, the gels were fixed and sectioned. (g, l) The invasion index was calculated and expressed as a ratio with respect to control cells treated with 0.005% DMSO. Results from three independent experiments are shown as means ± SD. $*P < 0.05$. Bar = 50 μm.

chain, which represents collective invasion by cancer cells (Fig. 3i). However, treatment of SAS cells with C-157 or D-572 effectively suppressed invasion (Fig. 3j–l).

C-157 and D-572 disrupted microtubules and prevented cancer cell invasion and growth. Next, we focused on two chemicals, C-157 and D-572, which showed the greatest inhibitory effects on cancer cell invasion. Compound C-157 is revealed as deoxypodophyllotoxin (DPT)[38] and D-572 is an indole alkaroid (Fig. 4a). Because cytoskeletal disturbance is one of the major causes of cell migration defects, the structure of microtubules was examined at first by immunostaining of SAS cells with anti-tubulin antibody. Microtubules were disrupted by C-157, which is reported in other cancer cells (Fig. S4).[39] Disruption of microtubule filaments in interphase was also observed by exposure to D-572 (Fig. S4). These observations strongly suggest that both C-157 and D-572 affect cell migration largely depending on the disruption of microtubule assembly.

Because microtubules also regulate cell mitosis, the effects of C-157 and D-572 on cell division, apoptosis and proliferation were further analyzed. When distribution of chromosomes in mitotic phase was compared in SAS cells, alignment of chromosomes in the central region at metaphase was not observed by treatment with these chemicals because of the disruption of spindle microtubules; instead, hyper-condensed chromosomes were detected, which are frequently observed in cells with mitotic arrest, typically induced by nocodazole treatment (Fig. 4b, Fig. 4e right). Addition of C-157 and D-572 increased rounded cells, which is a distinctive feature of mitotic cells (Fig. 4c). Increase in mitotic cells by C-157 and D-572 was further confirmed by the observation that the rate of cells with condensed (Fig. 4d, arrows) or hyper-condensed (Fig. 4d, arrowheads) chromosomes was increased by these compounds (Fig. 4d–f). Although the effect of D-572 was weaker than C-157, a statistically significant increase of mitotic cells was observed. Live-imaging of these cells revealed the prolonged mitotic phase by C-157 and D-572, which normally finished within 1 h (Fig. 4g). These results suggest that C-157 and D-572 blocked the progression of mitotic phase by inhibition of spindle formation.

When the effects of these chemicals on SAS cell apoptosis were examined, we found that both increased apoptosis; however, C-157 was more effective than D-572 (Fig. 5a, left). The half maximal inhibitory dose (IC50) value of C-157 and D-572 was 0.3 μM and 2.0 μM, respectively. Dose-dependent apoptosis induced by D-572 was also confirmed by labeling SAS cells with Hoechst 33342 (Fig. 5a, right panels). The MTT

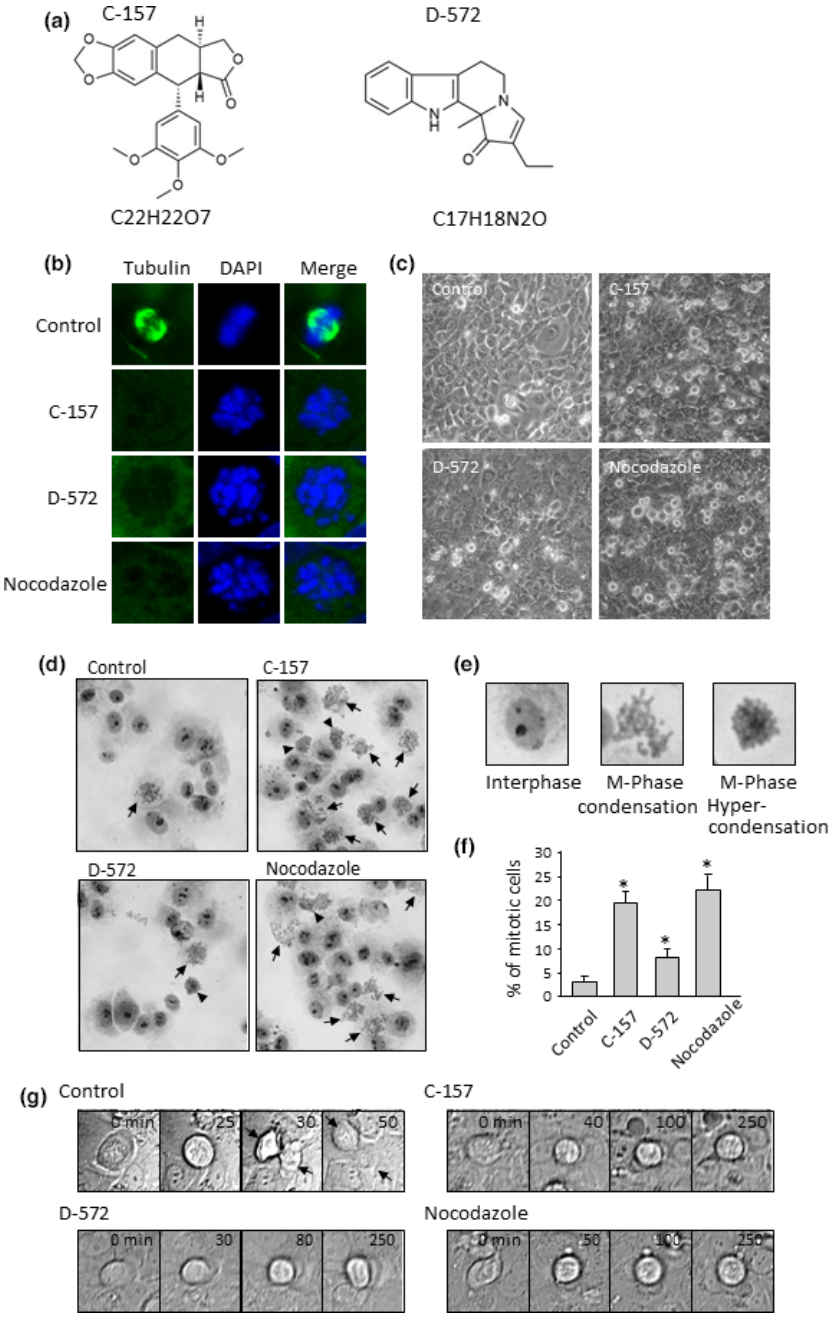

Fig. 4. C-157 and D-572 cause mitotic defect in SAS cells. (a) The structure of C-157 and D-572. (b–f) All experiments were observed at 15 h after addition of C-157 and D-572 (10 μM, each) or nocodazole (2 μM). (b) SAS cells were fixed with methanol and stained with α-tubulin antibody (green). DNA was stained with DAPI (blue). Panels show spindle microtubules in control cells at metaphase and disrupted microtubules in drug-treated cells at prometaphase. (c) Phase-contrast microscope images in control and drug-treated SAS cells. (d) Giemsa staining of control and drug-treated SAS cells. After addition of each drug, cells were fixed with methanol/acetic acid and then stained by Giemsa solution. Arrows and arrowheads indicate the chromosome condensation and hyper-condensation in mitotic phase, respectively. (e) Enlargement of interphase or mitotic cells in (d). (f) Frequency (%) of mitotic cells after C-157 or D-572 treatment. Mitotic cells were discriminated by the chromosome condensation as shown in (e) by Giemsa staining. $*P < 0.05$. (g) Live cell imaging of mitosis in SAS cells. Arrows in control cells indicate the daughter cells created by cell division. "Time 0" was defined as the onset of prophase.

assay revealed that C-157 reduced the viability of SAS cells in a dose-dependent manner (Fig. 5b). By contrast, D-572 had little effect on the viability of SAS cells within 12 h (Fig. 5b). We could not evaluate higher concentrations because D-572 was insoluble in culture medium at high doses. Taken together, these results indicate that C-157 and D-572 affected cell mitosis and induced apoptosis in SAS cells.

Both C-157 and D-572 suppressed Akt and Erk, two major molecules regulating cell survival and growth, but with different specificity. Addition of C-157 (1 μM) to SAS cells effectively abolished activation of both Akt and Erk. In contrast, the inhibitory effect of D-572 on Akt activation was not significant (Fig. 5c).

Suppression of growth and invasion of xenograft tumors by C-157 and D-572. To assess whether C-157 and D-572 affect the growth of SAS tumors, SAS cells were injected subcutaneously into nude mice. The mice were then intratumoral injected with C-157 or D-572 (20 μM) (Fig. 6a, top). The mean weight of the subcutaneous tumors injected with C-157 and D-572 was reduced to 25% and 65%, respectively, that of control tumors (Fig. 6a). Histologic examination revealed that a large part of the tumor injected with C-157 was replaced by granulation tissue (Fig. 6b).

Next, we examined the effect of the compounds on the peritoneal dissemination of Axcel melanoma cells. Axcel cells were injected intraperitoneally in nude mice, followed by the compounds on days 5, 10 and 15 (Fig. 6c, top). When peritoneal dissemination in control and treated mice was compared at 20 days after cancer cell injection, we found that both the number and size of the tumors in the mesentery of mice

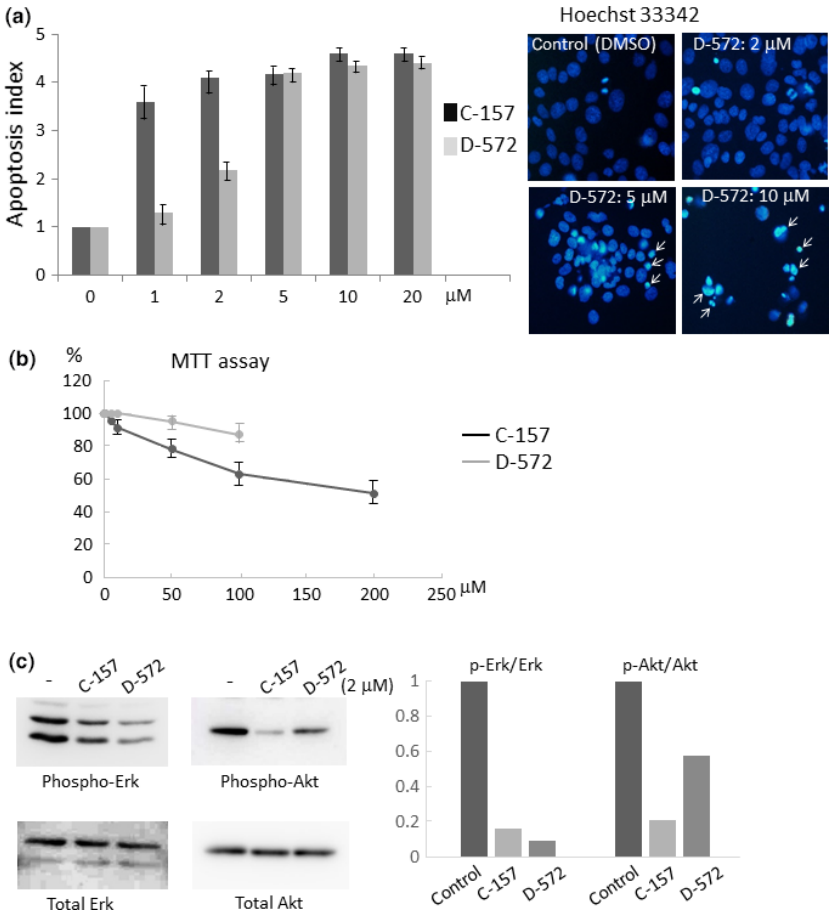

Fig. 5. Effects of C-157 and D-572 on apoptosis and viability of SAS cells. (a, b) Apoptosis and viability of SAS cells after treatment with chemicals. The results from triplicate samples are shown as the means ± SD. (b, right panels) SAS cells were labeled with Hoechst 33342, and treated with chemicals. Arrows indicate representative apoptotic cells containing condensed or fragmented nucleus. (c) Western blot analysis of SAS cell lysates with antibodies against phosphorylated and total Erk and Akt. The intensity of each band was measured by ImageJ software and the relative ratio of phosphorylated-to-total Erk or Akt was calculated.

treated with C-157 and D-572 were lower (Fig. 6c). Moreover, the anti-tumor effects of the compounds were examined in brain tumors formed by a glioblastoma cell line. Intracranial injection of C6 glioblastoma cells followed by injection of C-157 and D-572 at the same site on day 5 led to a significant reduction in tumor cell migration into the surrounding brain tissue at day 9. The tumor margin in control mice was irregular, whereas that in mice treated with C-157 or D-572 was well demarcated, with a clear margin (Fig. 6d).

Discussion

Here, using Xenopus embryos, we aimed to identify chemical compounds that affect invasion by cancer cells. We blindly screened 100 synthesized chemical compounds *in vivo* by evaluating gastrulation and NCC migration, and selected nine compounds that affect migration and invasion during at least one of these developmental events. Among these, C-157 and D-572 inhibited the invasion as well as proliferation of several types of cancer cells. Microtubules are required for interphase functions, including maintenance of cell shape and motility, and are also important for the function of mitotic spindle. As expected from the result that Paclitaxel, a cytoskeletal drug targeting microtubules, was selected by this screening, compounds like C-157 and D-572 that also affect cell proliferation depending on mitotic defects via microtubule disturbance were identified. Therefore, our *in vivo* screening method is useful for identifying compounds that suppress cancer invasion and/or proliferation. In additionm it is effective for detection of compounds like AMD3100 that perturb cell migration based on SDF1-CXCR4 signaling.

The anti-tumor effect of DPT is well studied, including its ability to increase apoptosis by inducing G2/M-phase arrest.[39–41] In addition, the antiangiogenic effect of DPT may also contribute to the significant reduction of tumor size of SAS cells.[42,43] D-572 also disrupted microtubules, and prevented the progression of mitotic phase, which was evident from the live-cell imaging. The effects by C-157 and D-572 seem to be different from that by Paclitaxel, as C-157 and D-572 destabilized microtubules, as judged from the immunostaining that microtubule filaments were not formed, whereas Paclitaxel prevents disassembly of microtubules.[35] However, all these agents inhibit normal mitotic phase progression and suppress cell proliferation. Because actively migrating cells may be more sensitive to the microtubule destabilizer or agents controlling the cell cycle than static cells, anti-tumor chemicals affecting the cell cycle can also be picked up by this approach. We initially expected that compounds preventing EMT were also selected from this screening. However, evident change of expression of EMT-marker genes, including snail, slug, E-cadherin and N-cadherin, was not detected in SAS cells by treatment with C-157 or D-572 (data not shown). This may be due to the timing of when these compounds were added. Because we added chemicals at stage 10, the onset of gastrulation, EMT had already progressed. In future, this screening should be improved by earlier exposure of embryos with testing compounds to identify EMT-interfering compounds.

Retrospectively, two compounds of podophyllotoxin-derivatives, C-162 and C-290, and two analogues of D-572, E-030 and GO-1523, were included in the chemical library (Figs S5a, S6a). However, they did not clearly affect gastrulation, and C-162 only weakly affected CNCC migration. Consistently, morphological change and the inhibitory effect on gel invasion

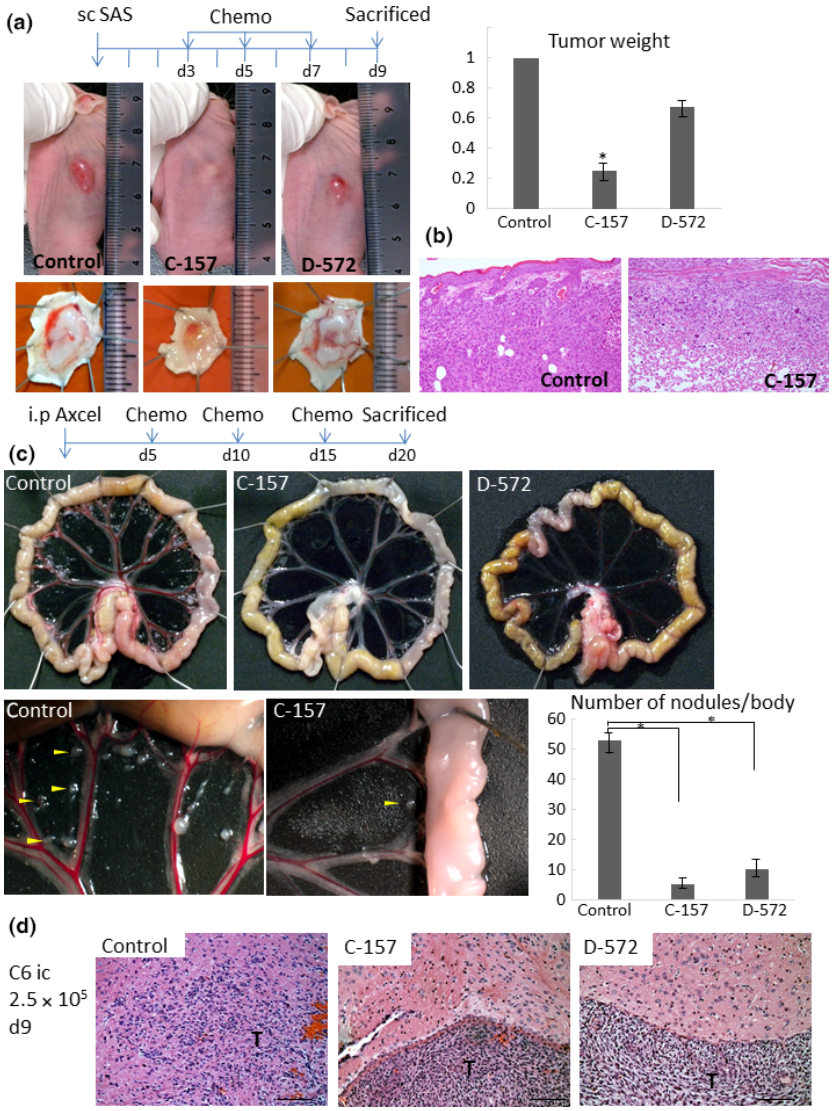

Fig. 6. Effects of C-157 and D-572 on tumor growth and invasion. (a) SAS cells were injected subcutaneously in nude mice and each compound (20 μM in 50 μL PBS) was injected three times at the same site as depicted. (b) Tumors were sectioned and subjected to HE staining. (c) Axcel cells were injected into the peritoneal cavity, followed by test chemicals (20 μM, 200 μL) as indicated. Arrow heads indicate disseminated tumors in the mesentery. The number of tumor nodules (>1 mm in diameter) in the mesentery was counted. (d) C6 cells were injected intra-cranially into nude mice, and test compounds (20 μM, 20 μL) were injected as described in the text. Representative histology of the mouse cerebrum at 9 days post-injection of tumor cells (H&E stain). T indicates the area occupied by tumor cells. (a–d) Five mice per each group were analyzed. Results are shown as means ± SD. $*P < 0.05$. Bar = 100 μm.

of SAS cells were weak by these compounds compared to C-157 or D-572, indicating that the anti-tumor effect was correlated with the inhibitory effect on embryonic development (Figs S5b,c, S6b). It is possible that other compounds selected from the Xenopus screening may affect the invasion or growth by other types of cancers. Further analysis by a series of cancer cells is also necessary to determine the false-positive rate; effective only in embryos, but not in cancer cells.

Xenopus produces a large number of oocytes (approximately 1000 at once), and artificially fertilized embryos show rapid gastrulation and migration of CNCC at 14 h and 34 h after fertilization at room temperature, respectively. To improve the efficiency of evaluating CNCC migration, the first round of *in situ* hybridization was performed by combining embryos from 3 to 5 different chemical treatment. Xenopus embryos are useful for screening chemical compounds that affect tumor growth and invasion. Although biological behaviors of embryonic cells and cancer cells are not identical, common pathways and molecules beyond the species could have critical roles in tumor biology. Future studies will involve screening on a larger scale to identify anti-tumor compounds that are both less toxic and more effective *in vivo*.

Acknowledgments

This work was supported by JST KAKENHI (Grant Nos. 25290042, 26640068 to M.T.; 15K06822 to S.K.), JST A-STEP (AS262Z01408Q to M.T.) and MEXT KAKENHI (25111702 to S.K.).

Disclosure Statement

The authors have no conflicts of interest to declare.

References

1 Friedl P, Hegerfeldt Y, Tusch M. Collective cell migration in morphogenesis and cancer. *Int J Dev Biol* 2004; **48**: 441–9.
2 Wolf K, Wu YI, Liu Y *et al.* Multi-step pericellular proteolysis controls the transition from individual to collective cancer cell invasion. *Nat Cell Biol* 2007; **9**: 893–904.
3 Friedl P, Gilmour D. Collective cell migration in morphogenesis, regeneration and cancer. *Nat Rev Mol Cell Biol* 2009; **10**: 445–57.
4 Munoz-Soriano V, Belacortu Y, Paricio N. Planar cell polarity signaling in collective cell movements during morphogenesis and disease. *Curr Genomics* 2012; **13**: 609–22.
5 Hardwick LJ, Philpott A. An oncologist's friend: how Xenopus contributes to cancer research. *Dev Biol* 2015; **408**: 180–7.

6 Gross SD, Schwab MS, Taieb FE, Lewellyn AL, Qian YW, Maller JL. The critical role of the MAP kinase pathway in meiosis II in Xenopus oocytes is mediated by p90 (Rsk). *Curr Biol* 2000; **10**: 430–8.
7 Favata MF, Horiuchi KY, Manos EJ *et al.* Identification of a novel inhibitor of mitogen-activated protein kinase kinase. *J Biol Chem* 1998; **273**: 18623–32.
8 Ogata S, Morokuma J, Hayata T *et al.* TGF-beta signaling-mediated morphogenesis: modulation of cell adhesion via cadherin endocytosis. *Genes Dev* 2007; **21**: 1817–31.
9 Fukui A, Goto T, Kitamoto J, Homma M, Asashima M. SDF-1 alpha regulates mesendodermal cell migration during frog gastrulation. *Biochem Biophys Res Commun* 2007; **354**: 472–7.
10 Libura J, Drukala J, Majka M *et al.* CXCR4-SDF-1 signaling is active in rhabdomyosarcoma cells and regulates locomotion, chemotaxis, and adhesion. *Blood* 2002; **100**: 2597–606.
11 Taichman RS, Cooper C, Keller ET, Pienta KJ, Taichman NS, McCauley LK. Use of the stromal cell-derived factor-1/CXCR4 pathway in prostate cancer metastasis to bone. *Cancer Res* 2002; **62**: 1832–7.
12 Zeelenberg IS, Ruuls-Van Stalle L, Roos E. The chemokine receptor CXCR4 is required for outgrowth of colon carcinoma micrometastases. *Cancer Res* 2003; **63**: 3833–9.
13 Fernandis AZ, Prasad A, Band H, Klosel R, Ganju RK. Regulation of CXCR4-mediated chemotaxis and chemoinvasion of breast cancer cells. *Oncogene* 2004; **23**: 157–67.
14 Kijima T, Maulik G, Ma PC *et al.* Regulation of cellular proliferation, cytoskeletal function, and signal transduction through CXCR4 and c-Kit in small cell lung cancer cells. *Cancer Res* 2002; **62**: 6304–11.
15 Mishra SK, Nagata T, Furusawa K, Sasaki A, Fukui A. Expression of xSDF-1alpha, xCXCR4, and xCXCR7 during gastrulation in *Xenopus laevis*. *Int J Dev Biol* 2013; **57**: 95–100.
16 Hara Y, Nagayama K, Yamamoto TS, Matsumoto T, Suzuki M, Ueno N. Directional migration of leading-edge mesoderm generates physical forces: implication in Xenopus notochord formation during gastrulation. *Dev Biol* 2013; **382**: 482–95.
17 Carmona-Fontaine C, Matthews HK, Kuriyama S *et al.* Contact inhibition of locomotion in vivo controls neural crest directional migration. *Nature* 2008; **456**: 957–61.
18 Kuriyama S, Mayor R. Molecular analysis of neural crest migration. *Philos Trans R Soc Lond B Biol Sci* 2008; **363**: 1349–62.
19 Theveneau E, Mayor R. Neural crest delamination and migration: from epithelium-to-mesenchyme transition to collective cell migration. *Dev Biol* 2012; **366**: 34–54.
20 Taneyhill LA, Coles EG, Bronner-Fraser M. Snail2 directly represses cadherin6B during epithelial-to-mesenchymal transitions of the neural crest. *Development* 2007; **134**: 1481–90.
21 Theveneau E, Marchant L, Kuriyama S *et al.* Collective chemotaxis requires contact-dependent cell polarity. *Dev Cell* 2010; **19**: 39–53.
22 Theveneau E, Steventon B, Scarpa E *et al.* Chase-and-run between adjacent cell populations promotes directional collective migration. *Nat Cell Biol* 2013; **15**: 763–72.
23 Kuriyama S, Theveneau E, Benedetto A *et al.* In vivo collective cell migration requires an LPAR2-dependent increase in tissue fluidity. *J Cell Biol* 2014; **206**: 113–27.
24 Fuyuhiro Y, Yashiro M, Noda S *et al.* Upregulation of cancer-associated myofibroblasts by TGF-β from scirrhous gastric carcinoma cells. *Br J Cancer* 2011; **105**: 996–1001.
25 Ubbels GA, Hara K, Koster CH, Kirschner MW. Evidence for a functional role of the cytoskeleton in determination of the dorsoventral axis in *Xenopus laevis* eggs. *J Embryol Exp Morphol* 1983; **77**: 15–37.
26 Kuriyama S, Lupo G, Ohta K, Ohnuma S, Harris WA, Tanaka H. Tsukushi controls ectodermal patterning and neural crest specification in Xenopus by direct regulation of BMP4 and X-delta-1 activity. *Development* 2006; **133**: 75–88.
27 Satoyoshi R, Kuriyama S, Aiba N, Yashiro M, Tanaka M. Asporin activates coordinated invasion of scirrhous gastric cancer and cancer associated fibroblasts. *Oncogene* 2015; **29**: 650–60.
28 Demetri GD, van Oosterom AT, Garrett CR *et al.* Efficacy and safety of sunitinib in patients with advanced gastrointestinal stromal tumour after failure of imatinib: a randomised controlled trial. *Lancet* 2006; **368**: 1329–38.
29 Motzer RJ, Hutson TE, Tomczak P *et al.* Overall survival and updated results for sunitinib compared with interferon alfa in patients with metastatic renal cell carcinoma. *J Clin Oncol* 2009; **27**: 3584–90.
30 Joensuu H. Sunitinib for imatinib-resistant GIST. *Lancet* 2006; **368**: 1303–4.
31 Simpson D, Keating GM. Sorafenib: in hepatocellular carcinoma. *Drugs* 2008; **68**: 251–8.
32 Takezawa K, Okamoto I, Yonesaka K *et al.* Sorafenib inhibits non-small cell lung cancer cell growth by targeting B-RAF in KRAS wild-type cells and C-RAF in KRAS mutant cells. *Cancer Res* 2009; **69**: 6515–21.
33 Sugiyama S, Yoshino Y, Kuriyama S *et al.* A curcumin analog, GO-Y078, effectively inhibits angiogenesis through actin disorganization. *Anticancer Agents Med Chem* 2016; **16**: 633–47.
34 Wani MC, Taylor HL, Wall ME, Coggon P, McPhail AT. Plant antitumor agents. VI. The isolation and structure of taxol, a novel antileukemic and antitumor agent from *Taxus brevifolia*. *J Am Chem Soc* 1971; **93**: 2325–7.
35 Rowinsky EK, Donehower RC. Paclitaxel (taxol). *N Engl J Med* 1995; **332**: 1004–14.
36 Rosenkilde MM, Gerlach LO, Jakobsen JS, Skerlj RT, Bridger GJ, Schwartz TW. Molecular mechanism of AMD3100 antagonism in the CXCR4 receptor: transfer of binding site to the CXCR3 receptor. *J Biol Chem* 2004; **279**: 3033–41.
37 Shindoh M, Higashino F, Kaya M *et al.* Correlated expression of matrix metalloproteinases and ets family transcription factor E1A-F in invasive oral squamous-cell-carcinoma-derived cell lines. *Am J Pathol* 1996; **148**: 693–700.
38 Takano S, Otaki S, Ogasawara K. Stereocontrolled synthesis of (±)-deoxypodophyllotoxin via the benzyl equivalent of the Peterson reaction. *J Chem Soc, Chem Commun* 1985; 485–7.
39 Guerram M, Jiang ZZ, Sun L, Zhu X, Zhang LY. Antineoplastic effects of deoxypodophyllotoxin, a potent cytotoxic agent of plant origin, on glioblastoma U-87 MG and SF126 cells. *Pharmacol Rep* 2015; **67**: 245–52.
40 Wang YR, Xu Y, Jiang ZZ *et al.* Deoxypodophyllotoxin induces G2/M cell cycle arrest and apoptosis in SGC-7901 cells and inhibits tumor growth in vivo. *Molecules* 2015; **20**: 1661–75.
41 Yong Y, Shin SY, Lee YH, Lim Y. Antitumor activity of deoxypodophyllotoxin isolated from *Anthriscus sylvestris*: induction of G2/M cell cycle arrest and caspase-dependent apoptosis. *Bioorg Med Chem Lett* 2009; **19**: 4367–71.
42 Sang CY, Xu XH, Qin WW, Liu JF, Chen SW. DPMA, a deoxypodophyllotoxin derivative, induces apoptosis and anti-angiogenesis in non-small cell lung cancer A549 cells. *Bioorg Med Chem Lett* 2013; **23**: 6650–5.
43 Jiang Z, Wu M, Miao J *et al.* Deoxypodophyllotoxin exerts both anti-angiogenic and vascular disrupting effects. *Int J Biochem Cell Biol* 2013; **45**: 1710–9.
44 Tanaka M, Wange L, Gupta R, Mayer BJ. Expression of mutated Nck SH2/SH3 adaptor respecifies mesodermal cell fate in *Xenopus laevis* development. *Proc Natl Acad Sci USA* 1997; **94**: 4493–8.

Supporting Information

Additional Supporting Information may be found online in the supporting information tab for this article:

Fig. S1. Supporting illustration of gastrulation.

Fig. S2. Evaluation of the screening system by known anti-cancer drugs.

Fig. S3. Additional images of 3D gel invasion assay.

Fig. S4. Cell morphology and immunostaining of microtubules in SAS cells.

Fig. S5. Comparison of C-157 and derivatives.

Fig. S6. Comparison of D-572 and analogues.

Data S1. Data for major chemical compounds used in this study.